Acta Mech 223, 2591–2596 (2012)
DOI 10.1007/s00707-012-0714-0

Qing Peng · Amir R. Zamiri · Wei Ji · Suvranu De

Elastic properties of hybrid graphene/boron nitride monolayer

Received: 12 November 2011 / Revised: 26 April 2012 / Published online: 16 September 2012

Abstract Recently, hybridized monolayers consisting of hexagonal boron nitride (*h*-BN) phases inside a graphene layer have been synthesized and shown to be an effective way of opening band gap in graphene monolayers (Ci et al. in Nat Mater 9(5):430–435, 2010). In this paper, we report a first-principles density functional theory study of the *h*-BN domain size effect on the elastic properties of graphene/boron nitride hybrid monolayers (*h*-BNC). We found that both in-plane stiffness and longitudinal sound velocity of *h*-BNC linearly decrease with *h*-BN concentration. Our results could be used for the design of future graphene-based nanodevices of surface acoustic wave sensors and waveguides.

1 Introduction

Substituting C with B and N atoms in graphene has been shown to be a promising way to improve semiconducting properties of graphene [2–4]. Hexagonal boron nitride (*h*-BN) monolayers [5] and graphene have similar 2D lattice structures but with very different physical properties. Interesting nanostructures can be made by mixing these two structures [6–9].

Recently, a promising method has been reported in which atomistic monolayers have been generated consisting of *h*-BN phases in graphene (*h*-BNC) using a thermal catalytic chemical vapor deposition method [1]. These hybrid monolayers have been shown to have isotropic physical properties that can be tailored by controlling the kinetic factors affecting the *h*-BN domain size within a graphene layer. This is different from B-doped or N-doped graphene, where the integrity of the *h*-BN structure is missing.

The electronic band structures of *h*-BNC heterostructures were studied in our previous work [10]. However, the mechanical properties of these heterogeneous nanosheets are still unknown. In this paper, we investigate the elastic properties of *h*-BNC monolayers as a function of *h*-BN concentration using *ab initio* density functional theory.

2 Modeling and computational details

The effect of the *h*-BN domain on the properties of the *h*-BNC hybrid structures is modeled by only considering the effect of its size while maintaining its hexagonal structure within the system. The *h*-BN domain size effect then can be represented by the *h*-BN concentration x in the model as $(B_3N_3)_x(C_6)_{1-x}$ where (B_3N_3) and (C_6) denote the nanodomain structure of the *h*-BN monolayer and the graphene, respectively. The proposed domain size effect model $(B_3N_3)_x(C_6)_{1-x}$ is based on the results of previous studies of $B_xC_yN_z$ layered

Q. Peng (✉) · A. R. Zamiri · W. Ji · S. De
Department of Mechanical, Aerospace and Nuclear Engineering,
Rensselaer Polytechnic Institute, Troy, NY 12180, USA
E-mail: pengq3@rpi.edu

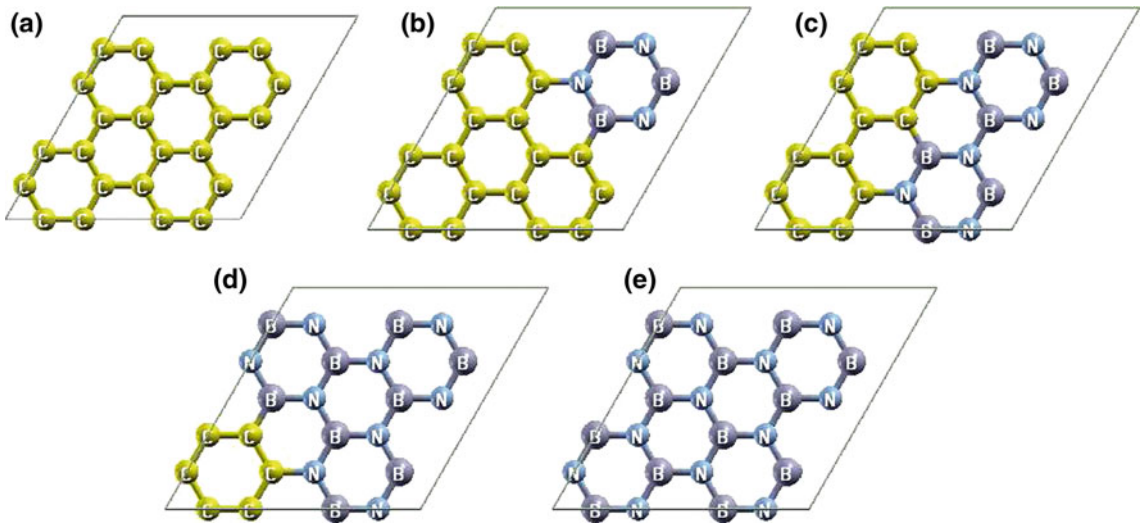

Fig. 1 Atomic structures of five configurations in order of *h*-BN concentration: **a** 0 %; **b** 25 %; **c** 50 %; **d** 75 %; **e** 100 %

structures [11], layers and nanotubes [12,13], quantum dots and nanorods [14], and monolayer nanohybrids [15]. It is a general belief that the *h*-BN segregates in the *h*-BNC, and the system gains lower energy, larger band gap, and better thermal stability after phase segregation [1,12,15]. The six-atom hexagonal structures (both B_3N_3 and C_6) are the basic blocks in these heterostructures. This model of $(B_3N_3)_x(C_6)_{1-x}$ captured the main feature of these heterostructures. As shown in previous works [11,12], both stoichiometry and geometry change the band gap of a B–C–N nanotube. The maximum band gap is achieved at a B/N ratio of 1. In the B–C–N monolayer, however, the domain size is a dominant factor compared to the domain shape in changing the band gap [15]. By varying the *h*-BN concentration x, the domain size effect on mechanical properties of monolayer hexagonal BNC heterostructures can be appropriately represented in our $(B_3N_3)_x(C_6)_{1-x}$ model.

We need to emphasize that although we only investigated the effect of stoichiometry of *h*-BN here, this domain model is different from a point model of $B_xC_yN_z$ at $x = z$ where the hexagonal (B_3N_3) structure is not considered [11]. In other words, our model specifies not only the stoichiometry of a B/N ratio of 1, but also the hexagonal (B_3N_3) and C_6 structures, to represent the two separated phases in heterogeneous *h*-BNC structures.

We examined the change in elastic properties of the *h*-BNC monolayer as a function of *h*-BN concentration. Five *h*-BNC configurations, in order of *h*-BN concentration 0, 25, 50, 75, and 100 % were studied, where 0 and 100 % correspond to pure graphene and *h*-BN, respectively. The three other concentrations were selected based on their simplicity and representativeness. The atomic structures of these five configurations (Fig. 1) were determined by the *ab initio* density functional theory through geometry optimization.

DFT calculations were carried out with the Vienna Ab-initio Simulation Package (VASP) [16–19], which is based on the Kohn–Sham density functional theory (KS-DFT) [20,21] with the generalized gradient approximations as parameterized by Perdew, Burke, and Ernzerhof (PBE) for exchange-correlation functions [22]. The electrons explicitly included in the calculations were the $(2s^22p^2)$ electrons of carbon, the $(2s^22p^1)$ electrons of boron, and the $(2s^22p^3)$ electrons of nitrogen. The core electrons $(1s^2)$ of carbon, boron, and nitrogen were replaced by the projector augmented wave (PAW) and pseudopotential approach [23,24]. A plane-wave cutoff of 520 eV was used in all the calculations; such value was chosen to eliminate the pulay stress during the geometry optimization [25].

The criterion for stopping the relaxation of the electronic degrees of freedom was set by the total energy change being smaller than 1.0–6 eV. The optimized atomic geometry was achieved through minimizing Hellmann-Feynman forces acting on each atom until the maximum forces on the ions were smaller than 0.001 eV/Å.

The atomic structures of the five configurations were obtained by fully relaxing a 24-atom-unit cell where all atoms were placed in one plane. The irreducible Brillouin zone was sampled with a Gamma-centered $19 \times 19 \times 1$ k-mesh, and initial charge densities were taken as a superposition of atomic charge densities. There was a 14 Å thick vacuum region to reduce the inter-layer interaction to model the single layer system.

The elastic tensors were determined by performing finite distortions of the lattice and deriving the elastic constants from the stress–strain relationships [26]. In this study, we were interested only in the in-plane

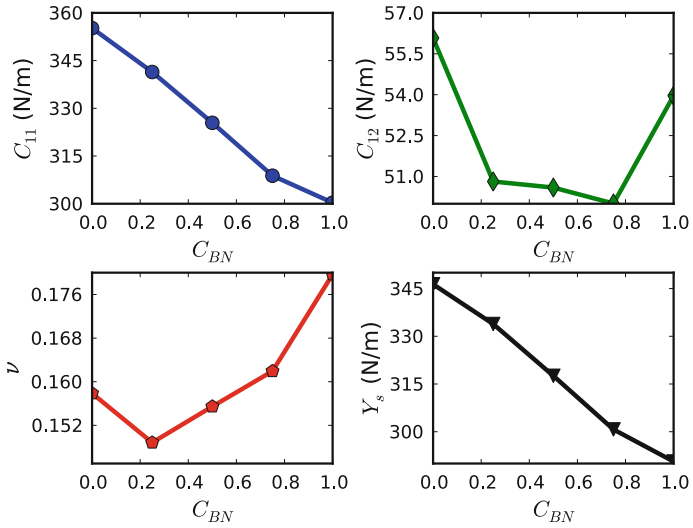

Fig. 2 Elastic constants C_{11} and C_{12}, Poisson's ratio ν and in-plane stiffness Y_s as a function of h-BN concentrations C_{BN}

elasticity. The strains of ± 0.015 were applied along two directions, x and xy. Two stress–strain curves, σ_{11} versus ε_{11} and σ_{12} versus ε_{12}, were computed, where σ_{11} and ε_{11} are stress and strain in xx direction, respectively, and σ_{12} and ε_{12} are the stress and strain in the xy direction. The elastic constants then were obtained through the least-squares extraction of coefficients from calculated stress–strain data. The final results of the values of these elastic constants were printed directly in VASP [26].

3 Results and analysis

With the full geometry optimization, including allowing the change of shape, the final atomic structures of the five configurations were determined using DFT calculations, as shown in panels (a)–(e) in Fig. 1. The hexagonal structures were still kept, even for the configuration (c), which has 50 % h-BN. In addition, we tested another atomic structure of configuration (c), where the two graphene rings were placed along the diagonal, instead of in parallel along the sides of supercell. The lattice constants of the two atomic structures are the same after geometry optimization, since the two atomic structures are symmetrical, and both have one layer of graphene ribbon in addition to one layer of h-BN ribbon, due to the periodic boundary conditions.

The lattice constants of the h-BNC mixtures were calculated as half of the lattice vectors of the supercells, for the convenience of comparison to those of the pure graphene and h-BN. We found that the lattice constant increases with h-BN concentration, which is denoted as C_{BN} in this paper. Our results are in a good agreement with previous experimental results reported for h-BN (2.51 Å) [27] and graphene (2.46 Å) [28].

The elastic constants were obtained from DFT calculations. Due to the symmetry, only C_{11} and C_{12} are independent. C_{11} decreases linearly with respect to C_{BN}, as plotted in the top-left panel of Fig. 2. The in-plane stiffness Y_{s} can be obtained from the elastic moduli C_{11} and C_{12} as $Y_{\mathrm{s}} = (C_{11}^2 - C_{12}^2)/C_{11}$. The Poisson's ratio ν which is the ratio of the transverse strain to the axial strain can be obtained from elastic moduli as $\nu = C_{12}/C_{11}$. Our results of ν, C_{11}, and C_{12} for the five configurations are shown in the Fig. 2. Our calculated value for in-plane stiffness of graphene (347.2 N/m) is in good agreement with the experimental value (340 ± 50 N/m) [29] and theoretical predictions (348 N/m in ref. [30] and 335 N/m in ref. [31]). Our calculated value of Y_{s} for h-BN (291.3 N/m) agrees with the *ab initio* (GGA-PW91) prediction (267 N/m in ref. [31]). The calculated Poisson's ratio ν is 0.16 for graphene and 0.18 for h-BN, which both agree with reported values of 0.16 and 0.21, respectively [31].

As shown in Fig. 2, both the C_{11} and the in-plane stiffness decrease nearly linearly as the h-BN concentration increases. However, the C_{12} and Poisson's ratio show rather complicated behaviors. The similar trend of the C_{11} and the in-plane stiffness is due to the fact that C_{11} is the dominant factor in computing the in-plane stiffness, about six times bigger than C_{12}. For the same reason, the Poisson's ratio ν has a similar trend as C_{12}. Therefore, our analysis only focuses on the dominant factor C_{11}.

The mechanical behavior is ultimately determined by the electronic structures. For a better understanding of the mechanism of linear elastic properties with respect to C_{BN}, we studied the total electronic charge density

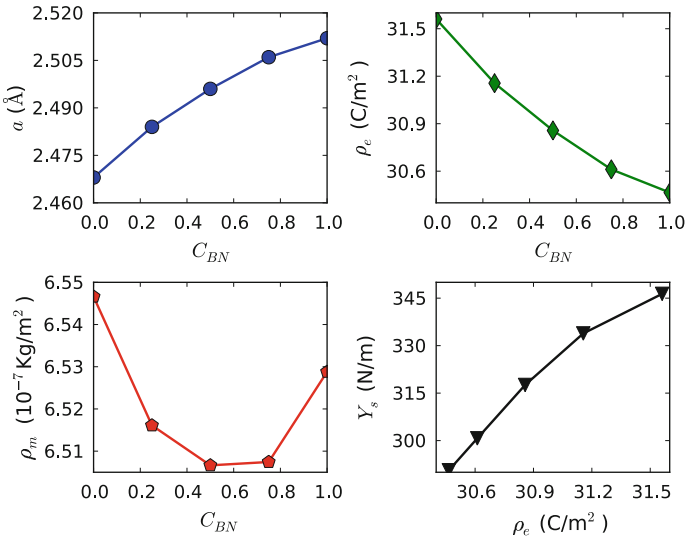

Fig. 3 Lattice constants a, electronic charge density ρ_{e}, and mass density ρ_{m} as a function of h-BN concentrations C_{BN}. The in-plane stiffness Y_{s} varied with electronic charge density is plotted

$\rho_{\mathrm{e}} = q/S$, where q is the total electronic charge of the system and S the area (cross-section) of the system in the basal plane. We found that ρ_{e} monotonically decreases with C_{BN}, as plotted in the top-right panel in Fig. 3. This relationship is consistent with the relation a-C_{BN}, since q is the same in all five configurations. The area mass density $\rho_{\mathrm{m}} = m/S$ (where m is the atomic mass) is also studied, as plotted in the bottom-left panel in Fig. 3. ρ_{m} reaches the minimum at $C_{\mathrm{BN}} = 0.5$.

The relationship between Y_{s} and ρ_{e} is plotted in the bottom-right panel of Fig. 3. It is interesting to note that the in-plane stiffness monotonically increases with respect to the area charge density ρ_{e}. This gives a hint that the elastic properties can be engineered by doping or introducing defects, which changes the charge densities.

In these h-BNC structures, there is a nonzero stiffness both for volumetric and shear deformations. Hence, it is possible to generate sound waves with different velocities dependent on the deformation mode. Sound waves generating volumetric deformations (compressions) and shear deformations are called longitudinal waves ($p-$wave) and shear waves ($s-$wave), respectively. The sound velocities of these two types of waves are, respectively, given by: [32]

$$v_p = \sqrt{\frac{Y_{\mathrm{s}}(1-\nu)}{\rho_{\mathrm{m}}(1+\nu)(1-2\nu)}}, \tag{1}$$

$$v_s = \sqrt{\frac{C_{12}}{\rho_{\mathrm{m}}}}. \tag{2}$$

The dependence of v_p and v_s on C_{BN} is plotted in Fig. 4. v_p monotonically reduced with C_{BN}. However, v_s has a more complex behavior. The v_s of h-BNC decreases with C_{BN}, but is lower than that of the pure phases, both graphene and h-BN. The v_p/v_s is in the range between 2.42 and 2.64.

Because the speed of these sound waves can be measured experimentally when these h-BNC heterostructures are synthesized, the predicted $p-$wave and $s-$wave velocities can serve as quantities validating the elastic properties.

Furthermore, we predicted a linear relationship between the sound velocity and the concentration of h-BN. As a result, a sound velocity gradient can be achieved by introducing h-BN domains into graphene. The sound velocity gradient can be used to form a sound frequency and ranging channel, which is the functional mechanism of surface acoustic wave (SAW) sensors and waveguides. Thus, graphene-based nanodevices of SAW sensors and waveguides can by synthesized with h-BNC for next-generation electronics.

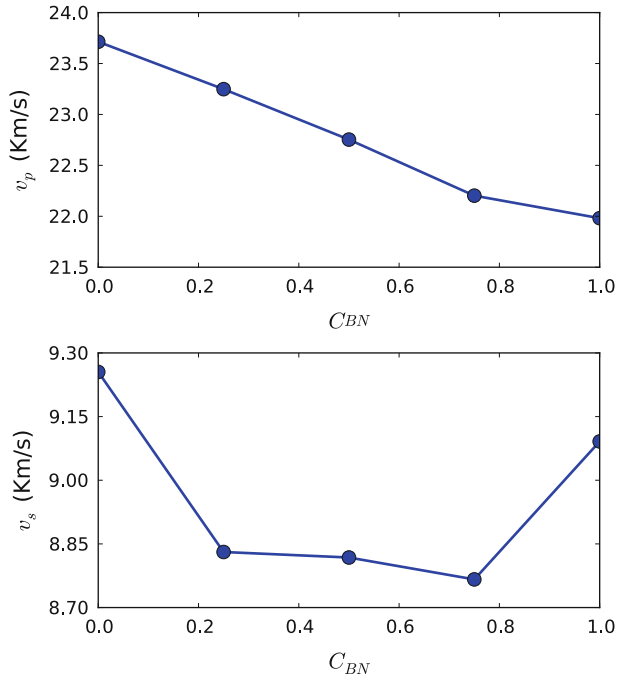

Fig. 4 $p-$wave and $s-$wave velocity as a function of h-BN concentrations C_{BN}

4 Conclusion

In summary, we used *ab initio* density functional theory to investigate the effect of the h-BN domain size on the elastic properties of graphene/h-BN hybrid monolayers. The elastic constants of five configurations were explicitly examined. We found that the in-plane stiffness increases linearly with the h-BN concentration. We predicted a linear relationship between the sound velocity and the concentration of h-BN. This knowledge could be used for the design of future graphene-based nanodevices of surface acoustic wave sensors and waveguides. Thus, our results may provide guidance in practical engineering applications of these nano-heterostructures.

Acknowledgments The authors would like to acknowledge the generous financial support from the Defense Threat Reduction Agency (DTRA) Grant # BRBAA08-C-2-0130.

References

1. Ci, L., Song, L., Jin, C., Jariwala, D., Wu, D., Li, Y., Srivastava, A., Wang, Z.F., Storr, K., Balicas, L., Liu, F., Ajayan, P.M.: Atomic layers of hybridized boron nitride and graphene domains. Nat. Mater. **9**(5), 430–435 (2010)
2. Wang, X., Li, X., Zhang, L., Yoon, Y., Weber, P.K., Wang, H., Guo, J., Dai, H.: N-doping of graphene through electrothermal reactions with ammonia. Science **324**(5928), 768 (2009)
3. Martins, T.B., Miwa, R.H., da Silva, A.J.R., Fazzio, A.: Electronic and transport properties of boron-doped graphene nanoribbons. Phys. Rev. Lett. **98**(19), 196803 (2007)
4. Lherbier, A., Blase, X., Niquet, Y.M., Triozon, F.M.C., Roche, S.: Charge transport in chemically doped 2d graphene. Phys. Rev. Lett. **101**(3), 036808 (2008)
5. Peng, Q., Ji, W., De, S.: Mechanical properties of the hexagonal boron nitride monolayer: Ab initio study. Comput. Mater. Sci. **56**, 11 (2012)
6. Kawaguchi, M., Kawashima, T., Nakajima, T.: Syntheses and structures of new graphite-like materials of composition BCN(h) and BC_3N(h). Chem. Mater. **8**(6), 1197–1201 (1996)
7. Suenaga, K., Colliex, C., Demoncy, N., Loiseau, A., Pascard, H., Willaime, F.: Synthesis of nanoparticles and nanotubes with well-separated layers of boron nitride and carbon. Science **278**(5338), 653–655 (1997)
8. Han, W.-Q., Mickelson, W., Cumings, J., Zettl, A.: Transformation of B[sub x]C[sub y]N[sub z] nanotubes to pure BN nanotubes. Appl. Phys. Lett. **81**(6), 1110–1112 (2002)
9. Kawasaki, T., Ichimura, T., Kishimoto, H., Akbar, A.A., Ogawa, T., Oshima, C.: Double atomic layers of graphene/monolayer h-BN on Ni(111) studied by scanning tunneling microscopy and scanning tunneling spectroscopy. Surf. Rev. Lett. **9**(3–4), 1459–1464 (2002)
10. Peng, Q., De, S.: Tunable band gaps of mono-layer hexagonal BNC heterostructures. Physica E **44**, 1776 (2012)

11. Mazzoni, M.S.C., Nunes, R.W., Azevedo, S., Chacham, H.: Electronic structure and energetics of $B_xC_yN_z$ layered structures. Phys. Rev. B **73**(7), 073108 (2006)
12. Martins, J.D.R., Chacham, H.: Disorder and segregation in B–C–N graphene- type layers and nanotubes: tuning the band gap. ACS Nano **5**(1), 385 (2011)
13. Bhowrnick, S., Singh, A.K., Yakobson, B.I.: Quantum dots and nanoroads of graphene embedded in hexagonal boron nitride. J. Phys. Chem. C **115**(20), 9889 (2011)
14. Singh, A.K., Yakobson, B.I.: Electronics and magnetism of patterned graphene nanoroads. Nano Lett. **9**(4), 1540–1543 (2009)
15. Manna, A.K., Pati, S.K.: Tunable electronic and magnetic properties in B(x)N(y)C(z) nanohybrids: effect of domain segregation. J. Phys. Chem. C **115**(21), 10842 (2011)
16. Kresse, G., Hafner, J.: Ab initio molecular dynamics for liquid metals. Phys. Rev. B **47**, 558 (1993)
17. Kresse, G., Hafner, J.: Ab initio molecular-dynamics simulation of the liquid-metalcamorphoussemiconductor transition in germanium. Phys. Rev. B **49**, 14251 (1994)
18. Kresse, G., Furthuller, J.: Efficient iterative schemes for ab initio total-energy calculations using a plane-wave basis set. Phys. Rev. B **54**, 11169 (1996)
19. Kresse, G., Furthuller, J.: Efficiency of ab-initio total energy calculations for metals and semiconductors using a plane-wave basis set. Comput. Mater. Sci. **6**, 15 (1996)
20. Hohenberg, P., Kohn, W.: Inhomogeneous electron gas. Phys. Rev. **136**(3B), B864 (1964)
21. Kohn, W., Sham, L.J.: Self-consistent equations including exchange and correlation effects. Phys. Rev. **140**(4A), A1133 (1965)
22. Perdew, J., Burke, K., Ernzerhof, M.: Generalized gradient approximation made simple. Phys. Rev. Lett. **77**, 3865 (1996)
23. Blöchl, P.E.: Projector augmented-wave method. Phys. Rev. B **50**(24), 17953–17979 (1994)
24. Jones, R.O., Gunnarsson, O.: The density functional formalism, its applications and prospects. Rev. Mod. Phys. **61**(3), 689–746 (1989)
25. Francis, G.P., Payne, M.C.: Finite basis set corrections to total energy pseudopotential calculations. J. Phys. Cond. Matter **2**(19), 4395–4404 (1990)
26. Le Page, Y., Saxe, P.: Symmetry-general least-squares extraction of elastic data for strained materials from ab initio calculations of stress. Phys. Rev. B **65**(10), 104104 (2002)
27. Liu, L., Feng, Y.P., Shen, Z.X.: Structural and electronic properties of h-BN. Phys. Rev. B **68**(10), 104102 (2003)
28. Baskin, Y., Meyer, L.: Lattice constants of graphite at low temperatures. Phys. Rev. **100**(2), 544 (1955)
29. Lee, C., Wei, X., Kysar, J.W., Hone, J.: Measurement of the elastic properties and intrinsic strength of monolayer graphene. Science **321**(5887), 385–388 (2008)
30. Wei, X., Fragneaud, B., Marianetti, C.A., Kysar, J.W.: Nonlinear elastic behavior of graphene: Ab initio calculations to continuum description. Phys. Rev. B **80**(20), 205407 (2009)
31. Topsakal, M., Cahangirov, S., Ciraci, S.: The response of mechanical and electronic properties of graphane to the elastic strain. Appl. Phys. Lett. **96**(9), 091912 (2010)
32. Kinsler, L.E.: Fundamentals of Acoustics. Wiley, New York (2000)